2020

Analysis of laminated composite plates with fluidstructure interaction using multiscale modeling technique

Kwon, Y.W.

Springer

http://hdl.handle.net/10945/65689

Multiscale and Multidisciplinary Modeling, Experiments and Design
https://doi.org/10.1007/s41939-020-00079-x

ORIGINAL PAPER

Analysis of laminated composite plates with fluid–structure interaction using multiscale modeling technique

Y. W. Kwon[1]

Received: 22 June 2020 / Accepted: 24 August 2020

Abstract
A series of numerical modeling and simulations were conducted to understand the dynamic response and failure of a laminated composite plate which was supported by water and subjected to dynamic loading. The structure was modelled using the plate/shell finite elements with displacements degrees of freedom only. The water medium was stationary and modelled as an acoustic domain using the cellular automata technique. The two analysis techniques were coupled for fluid–structure interaction (FSI). Composite materials were modelled using the multiscale approach. The constituent material-based failure criteria (i.e. in terms of fiber, matrix, and fiber/matrix interface failures) were used to predict failure of the fibrous composite. Failure of the same composite plate was investigated and compared when the plate was supported by water or not to understand the effect of the FSI between the composite plates and water on the dynamic response and failure. The numerical study showed that the dynamic response and failure of the composite plate were very dependent on FSI, and the numerical study qualitatively confirmed previous experimental studies.

Keywords Composite material and structure · Fluid–structure interaction · Multiscale analysis · Cellular automata · Failure analysis

1 Introduction

With the increase of composite materials for load-bearing structural components, more composites have been considered and applied for various engineering applications. More recently, composite materials have been also used for marine and offshore structures. One of the unique characteristics of such marine and offshore structures is the interaction of the structure and water, which is called the fluid–structure interaction (FSI).

There are various kinds of FSI problems. One of the industries which have been interested in FSI problems is the pressure vessels and piping industry. For example, sloshing of fluids in pressure vessels and flow-induced vibrations of pipes are some of the FSI problems (Weaver et al. 2000; Chen et al. 1996; Karamanos et al. 2006). Some other FSI problems were biomechanics (Di Martino et al. 2001; Simsek and Kwon 2015), and underwater explosion (Kwon and Fox 1993).

Impact studies were conducted extensively for composite structures (Abrate 1994; Aslan et al. 2003; Strait et al. 1992; Hosur et al. 2007). Most of those studies did not consider FSI. More recently, impact studies have been conducted for composite structures including the effect of FSI. Impact studies were conducted for various composite structures containing different amounts of water inside of them (Kwon and Bowling 2018; Kwon et al. 2017; Alaei et al. 2019). Those are the examples of fluids inside structures. However, most marine and offshore structures have fluids outside of the structures such as ships and offshore structures. Research was conducted for dynamic response and failure of composite structures submerged in water and subjected to impact loading (Kwon 2020; Kwon et al. 2010, 2012, 2013; Kwon and Violette 2012; Kwon and Conner 2012; Kwon and Plessas 2014). Other studies examined harmonic motions such as cyclic loading applied to composite structures with FSI (Kwon 2014; Kwon et al. 2016).

Most of the previous studies were experimental research. To the best knowledge of the author, there has been a very limited number of studies on numerical modeling and simula-

✉ Y. W. Kwon
ywkwon@nps.edu

[1] Department of Mechanical and Aerospace Engineering, Naval Postgraduate School, Monterey, CA 93943, USA

Published online: 06 September 2020

tion of composite structures for dynamic response and failure while the structures interact with a fluid medium, and subjected to impact loading (Kwon and Plessas 2014; Craugh and Kwon 2013). Thus, the objective of this study was to investigate the effect of FSI on dynamic response and failure of laminate composite plates. To this end, the numerical analyses were undertaken by coupling the finite element method (FEM) for the structural member and the cellular automata (CA) technique for the fluid domain. The dynamic response and failure were compared when a composite plate was subjected to the same loading, while one case included FSI and the other case excluded FSI.

The next sections discussed the finite element modeling of laminated composite structures using plate/shell finite elements with displacement degrees of freedom only, multiscale approach for composite modeling including the failure criteria based on the constituent level stresses and strains, and the cellular automata technique for modeling water as an acoustic domain with various boundary conditions. Then, numerical results and discussion were provided followed by conclusions.

2 Finite element for plate bending

This section describes the finite element formulation used in this study. The plate/shell elements with displacements degrees of freedom were used, because they have advantages for coupling with fluid domains for FSI analyses. Thus, the plate/shell element does not have rotational degrees of freedom. The element geometry looks like the same as traditional plate/shell elements, but the nodal degrees of freedom are different between the present and the traditional plate/shell elements.

Figure 1 shows the four-node plate/shell elements with nodal degrees of freedom (Kwon and Bang 2000; Kwon 2013). Each node has six degrees of freedom, two set in each direction of the three local coordinates. Two of them are in the inplane axes and the third one is in the transverse direction. The displacement field in the element is expressed as below:

$$u = \sum_{i=1}^{4} \Big(N_i(\xi, \eta) \Big(H_1(z) u_i^b + H_2(z) u_i^t \Big) \Big),$$
$$v = \sum_{i=1}^{4} \Big(N_i(\xi, \eta) \Big(H_1(z) v_i^b + H_2(z) w_i^t \Big) \Big),$$
$$w = \sum_{i=1}^{4} \Big(N_i(\xi, \eta) \Big(H_1(z) w_i^b + H_2(z) w_i^t \Big) \Big), \tag{1}$$

where u, v and w are the displacements in the x-, y- and z-axes, respectively, where the z-axis is the transverse normal axis.

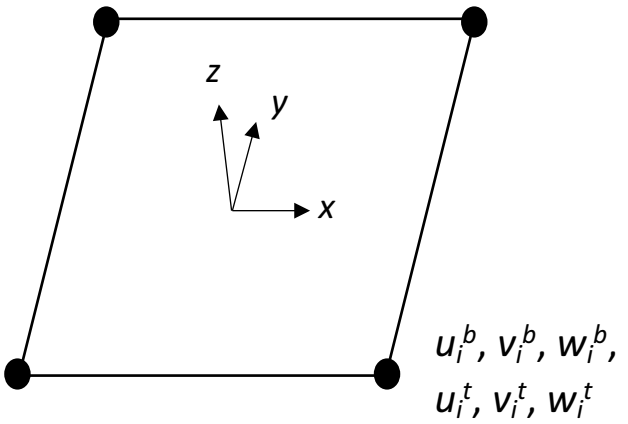

Fig. 1 Plate/shell element with six displacement degrees of freedom per node

The shape functions $N_i(\xi, \eta)$ is the 2-D isoparametric shape function for the four node element, and $H_1(z)$ and $H_2(z)$ are the linear shape functions along the thickness direction of the plate. While the Gauss quadrature integration is conducted over the inplane direction, the trapezoidal rule is used for the thickness direction. This is because the plate may be divided into many layers for the laminated composite plate. In addition, the superscripts b and t denote the bottom and top sides of the plate element.

The bending strains are expressed as below:

$$\varepsilon_x = \frac{\partial u}{\partial x} = \frac{\partial}{\partial x} \sum_{i=1}^{4} \Big(N_i(\xi, \eta) \Big(H_1(z) u_i^b + H_2(z) u_i^t \Big) \Big),$$
$$\varepsilon_y = \frac{\partial v}{\partial y} = \frac{\partial}{\partial y} \sum_{i=1}^{4} \Big(N_i(\xi, \eta) \Big(H_1(z) v_i^b + H_2(z) v_i^t \Big) \Big),$$
$$\gamma_{xy} = \frac{\partial u}{\partial y} + \frac{\partial v}{\partial x} = \frac{\partial}{\partial y} \sum_{i=1}^{4} \Big(N_i(\xi, \eta) \Big(H_1(z) u_i^b + H_2(z) u_i^t \Big) \Big) + \frac{\partial}{\partial x} \sum_{i=1}^{4} \Big(N_i(\xi, \eta) \Big(H_1(z) v_i^b + H_2(z) v_i^t \Big) \Big), \tag{2}$$

where ε_x, ε_y and γ_{xy} are two inplane normal and one inplane shear strains. Putting those expressions as a matrix equation yields the following expression

$$\{\varepsilon_b\} = [B_b]\{d\}, \tag{3}$$

in which $\{\varepsilon_b\}$ is the bending strains as below:

$$\{\varepsilon_b\} = \left\{ \varepsilon_x \ \varepsilon_y \ \gamma_{xy} \right\}^T, \tag{4}$$

and $\{d\}$ the nodal displacement vector of a single plate element as defined below:

$$\{d\} = \left\{ \{d_1\} \ \{d_2\} \ \{d_3\} \ \{d_4\} \right\}^T, \tag{5}$$

$$\{d_i\} = \left\{ u_i^b \;\; v_i^b \;\; w_i^b \;\; u_i^t \;\; v_i^t \;\; w_i^t \right\}. \tag{6}$$

The transverse shear strains are expresses as

$$\begin{aligned}
\gamma_{xz} &= \frac{\partial u}{\partial z} + \frac{\partial w}{\partial x} = \frac{\partial}{\partial z} \sum_{i=1}^{4} \left(N_i(\xi, \eta) \left(H_1(z) u_i^b + H_2(z) u_i^t \right) \right) \\
&\quad + \frac{\partial}{\partial x} \sum_{i=1}^{4} \left(N_i(\xi, \eta) \left(H_1(z) w_i^b + H_2(z) w_i^t \right) \right), \\
\gamma_{yz} &= \frac{\partial v}{\partial z} + \frac{\partial w}{\partial y} = \frac{\partial}{\partial z} \sum_{i=1}^{4} \left(N_i(\xi, \eta) \left(H_1(z) v_i^b + H_2(z) v_i^t \right) \right) \\
&\quad + \frac{\partial}{\partial y} \sum_{i=1}^{4} \left(N_i(\xi, \eta) \left(H_1(z) w_i^b + H_2(z) w_i^t \right) \right),
\end{aligned} \tag{7}$$

The expressions in Eq. (7) can be also rewritten in the matrix form as below:

$$\{\varepsilon_s\} = [B_s]\{d\}, \tag{8}$$

in which $\{\varepsilon_s\}$ is the transverse shear strains as below:

$$\{\varepsilon_b\} = \left\{ \varepsilon_{xz} \;\; \varepsilon_{yz} \right\}^T. \tag{9}$$

The element matrix for the plate bending is expressed as

$$\begin{aligned}
\left[K^e\right] &= \int_{-h/2}^{h/2} \int_{A^e} [B_b]^T [D_b] [B_b] \, \mathrm{d}A \mathrm{d}z \\
&\quad + \int_{-h/2}^{h/2} \int_{A^e} [B_s]^T [D_s] [B_s] \, \mathrm{d}A \mathrm{d}z.
\end{aligned} \tag{10}$$

Here $[D_b]$ and $[D_s]$ are the material property matrices for the bending and transverse shear components, respectively, which are discussed in the subsequent section. The element stiffness matrix of Eq. (10) does not provide a coupling between the top and bottom transverse displacements, i.e. w_i^b and w_i^t since the normal strain energy along the thickness direction is neglected. With the assumption that there is no deformation along the thickness, the penalty method is applied to w_i^b and w_i^t such that they are constrained to move together. An alternative is to reduce the transverse displacement into a single degree of freedom without applying the penalty method. However, in the present formulation, both transverse displacements were included. When a structure interacts with a fluid medium, the fluid may be on the bottom side, top side, or both sides. In those applications, independent displacements at the top and bottom sides of each plate element are useful for coupling with any fluid medium to conduct FSI analyses.

A laminated composite structure can be modelled using a couple of different ways. The simplest way is to model the whole laminate as a single plate/shell element. This is called the smeared model. Different layers are considered by the numerical integration points along the thickness direction. At least one integration point is assigned to each layer such that the layer orientation can be properly considered in the finite element formulation. This technique is equivalent to the Mindlin/Reissner bending theory. The inplane displacements vary linearly along the whole thickness. This technique is computationally the least expensive.

Another technique is each individual layer is modelled as a single plate/shell element. This is called the discrete model. Since the plate/shell elements have only displacement degrees of freedom, it is straightforward to assemble the elements along the thickness of the laminated structure. This modeling technique is similar to a higher order bending theory. In this model, inplane displacement can vary as a piecewise linear function along the structural thickness. This technique makes more degrees of freedom in the matrix equation, and this is computationally the most expensive. Another way of modelling is the combination of the two previous techniques. In other words, some layers are modelled using the individual plate/shell element while other layers are smeared into a single element. The computational cost is between the two previous cases. If a laminated composite structure consists of different composites from layer to layer, the discrete modeling of each layer is preferred.

3 Multiscale modeling of composite materials and failure

The multiscale technique was used to analyze the behavior of composite materials and their failure (Kwon 2016; Kwon and Darcy 2018a, b). The multiscale approach is to link the microscale and macroscale bi-directionally. In other words, the constituent materials like the fibers and matrix are connected to the composite material in both directions. The multiscale has the upscaling and downscaling processes. The upscaling process is to compute the effective composite material properties from the properties of the fiber and matrix materials. The upscaling is also called the stiffness procedure. The downscaling process is to decompose the stresses and strains at the composite material level into the stresses and strains at the fiber and matrix material level. The downscaling process is also called the strength procedure. The downscaling is important to apply failure criteria at the fiber and matrix material level rather than the composite material level. Figure 2 shows the overall schematics of the multiscale approach.

To undertake the multiscale approach, a unit-cell model was used which can provide information for both upscaling and downscaling processes (Kwon and Kim 1998; Kwon and Park 2013; Kwon 2016). The unit cell for the continuous

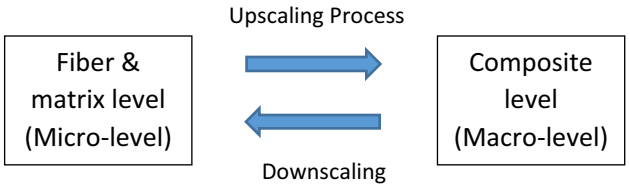

Fig. 2 Multiscale approach for fibrous composite material

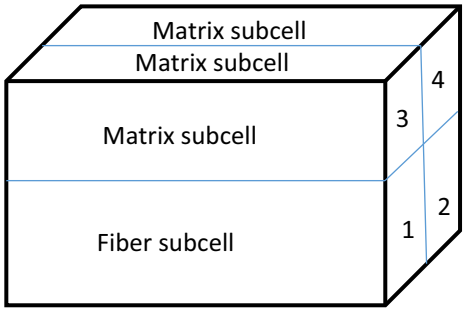

Fig. 3 Unit-cell model for fibrous composite

fiber composite consists of four subcells with symmetry as sketched in Fig. 3. One of the subcell represents the fiber material and the rest of subcells are the surrounding matrix material. The size of the fiber subcell is determined based on the fiber volume fraction of the composite. Thus, the fiber subcell does not represent a single fiber. Instead, it represents the average of collective fibers.

The detailed presentation and discussion of the unit-cell model was provided in previous publications (Kwon 2016; Kwon and Darcy 2018a; Kwon and Kim 1998; Kwon and Park 2013). Therefore, a brief explanation is given here for completeness. For mathematical simplicity, each subcell is assumed to have uniform stresses and strains. Then, the stresses and strains are related by the constitutive equations of the material, either the fiber or the matrix material. Furthermore, force equilibrium at the interface of every two neighboring subcells is applied in terms of the stress components at the subcells. Both normal and tangential forces should be equilibrated. In addition, strains should maintain deformation compatibility. Finally, the composite level stresses and strains are assumed to be the volume average of subcell level stresses and strains. Proper manipulation of those equations provides the following two main mathematical equations.

$$[E^c] = f\left(\left[E^f\right], \left[E^m\right], v^f, v^m\right), \tag{11}$$

$$\left\{\varepsilon^f \text{ and } \varepsilon^m\right\} = [R]\left\{\varepsilon^c\right\}. \tag{12}$$

Equation (11) is used for the upscaling process. That is, the composite material property $[E^c]$ is computed from the material properties of the fiber $\left[E^f\right]$ and the matrix $\left[E^m\right]$ as well as their volume fractions v^f and v^m. Here superscripts c, f and m denote the composite, fiber and matrix materials. If there is no void, $v^f + v^m = 1$. Equation (12) is used for the downscaling process. The fiber and matrix level strains are computed from the composite level strains determined from the finite element analysis. Once strains are computed for the fiber and matrix materials, the corresponding stresses are computed from the strains using the appropriate constitutive equations of the fiber and matrix materials.

Once the stresses and strains are computed for the fiber and matrix materials, failure criteria are applied at the fiber and matrix level using the stresses and strains. The failure criteria consist of three main failure modes; fiber failure, matrix failure, and fiber/matrix interface failure (Kwon and Darcy 2018a, b; Kwon and Panick 2020). The fiber failure may be either in tensile fracture or compressive buckling. Depending on the nature of the material behavior of the fiber and matrix, appropriate failure criteria can be selected and used. For the present study, brittle fiber and matrix materials were considered.

The fiber failure criterion is expressed as below:

$$\sqrt{\left(\varepsilon_1^f\right)^2 + \left(\gamma_{12}^f\right)^2 + \left(\gamma_{13}^f\right)^2} \geq \varepsilon_{\text{fail}}^f, \tag{13}$$

where $\varepsilon_{\text{fail}}^f$ is the fiber failure strain. The failure strain may be different for tensile or compressive loading, and the proper failure strain should be used depending on the tensile or compressive strain. In this expression, subscript 1 is the fiber orientation.

The matrix was assumed to be isotropic and brittle. Thus, the maximum strain criterion is used for the matrix failure as expressed below:

$$\varepsilon_{p1}^m \geq \varepsilon_T^m \text{ or } \left|\varepsilon_{p3}^m\right| \geq \left|\varepsilon_C^m\right|. \tag{14}$$

where ε_{p1}^m is the largest positive principal strain in the matrix, and ε_{p3}^m is the largest magnitude of the negative principal strain. If the failure strain is the same under tensile and compressive loading, $\varepsilon_T^m = \left|\varepsilon_C^m\right|$.

The last failure criterion is for the fiber/matrix interface debonding. In a simplified case, the matrix failure criterion was considered for the fiber/matrix debonding. However, previous studies suggested that the interface failure was very different from the matrix failure. The proposed interface failure criterion is

$$\left(\frac{\tau^{\text{int}} + \sqrt{v^f}\left(\sigma_2^m - \sigma_1^m\right)}{\tau_{\text{fail}}^{\text{int}}}\right)^2 + \left\langle\frac{\sigma_2^m}{\sigma_{\text{fail}}^{\text{int}}}\right\rangle^2 \geq 1, \tag{15}$$

where $\langle a\rangle = \frac{a+|a|}{2}$ is the Macaulay operator. In addition, $\tau_{\text{fail}}^{\text{int}}$ and $\sigma_{\text{fail}}^{\text{int}}$ are the failure strength under shear and normal

loads, respectively. The superscripts *int* and *m* indicate the interface and the matrix material.

Once the fiber and/or matrix material fails at a numerical integration point, the corresponding material properties are degraded accordingly, and the analysis continues until there is the major failure such that the structure cannot support the applied loading any longer. This is manifested by an unexpected large strains or deformations in the structure. Reference (Kwon and Darcy 2018b) provided the detailed algorithms to model the progressive damage until final failure.

4 Cellular automata technique for fluid domain

The fluid domain was modeled as an acoustic domain by neglecting any fluid motion. Hence, the wave equation was used for the fluid domain as given below:

$$\frac{\partial^2 p}{\partial t^2} = c^2 \nabla^2 p, \tag{16}$$

in which p and c are the acoustic pressure and the wave speed, respectively. The cellular automata (CA) technique uses the same set of rules at every cell or grid point repeatedly. To this end, the necessary mathematical rules are developed using the finite difference technique. Those are shown below (Kwon 2017):

$$\begin{aligned}
\ddot{p}^t_{i,j,k} &= c^2 \left(p^t_{i+1,j,k} + p^t_{i-1,j,k} - 2p^t_{i,j,k} \right) / (\Delta x)^2 \\
&\quad + c^2 \left(p^t_{i,j+1,k} + p^t_{i,j-1,k} - 2p^t_{i,j,k} \right) / (\Delta y)^2 \\
&\quad + c^2 \left(p^t_{i,j,k+1} + p^t_{i,j,k-1} - 2p^t_{i,j,k} \right) / (\Delta z)^2 , \\
\dot{p}^{t+\Delta t}_{i,j,k} &= \dot{p}^t_{i,j,k} + \ddot{p}^t_{i,j,k} (\Delta t) , \\
p^{t+\Delta t}_{i,j,k} &= p^t_{i,j,k} + \dot{p}^{t+\Delta t}_{i,j,k} (\Delta t) .
\end{aligned} \tag{17}$$

The boundary conditions can be explained in terms of the one-dimensional perspective since the same condition can be applied to either 2-D or 3-D domains without any change. Let's consider the leftmost grid p_1 as the boundary point. Because the non-reflective boundary condition was used in this study, that boundary condition is described here. The non-reflective boundary is applied using the following expression:

$$p_0 = (p_2 - p_1)/\alpha - p_2 + 2p_1 \text{ and } \dot{p}_1 = 0, \tag{18}$$

where

$$\alpha = \frac{c^2 \Delta t^2}{\Delta x^2}. \tag{19}$$

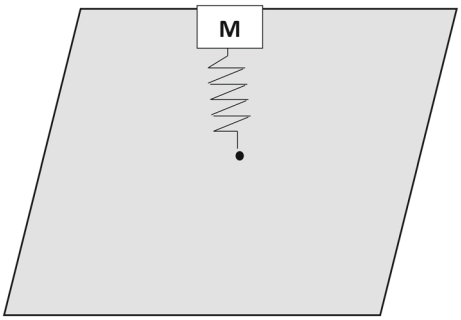

Fig. 4 Simplified model of rigid mass impact to plate

If $\Delta x/\Delta t = c$, α becomes unity. Then, Eq. (18) is simplified to

$$p_o = p_1, \ \dot{p}_1 = 0. \tag{20}$$

As the acoustic domain has an interface with the structural domain for an FSI analysis, a proper set of interface conditions must be applied at the interface. In other words, proper equilibrium and continuity conditions should be maintained at the interface. One of the conditions is that the pressure should be the same between the acoustic and structural domain at the interface. The second condition is the motion should be continuous at the interface. Because the acoustic domain has pressure at the grid point while the structural domain has displacement, velocity, and acceleration at the nodal point; the compatibility equation is

$$\frac{\partial p}{\partial n} = \rho \ddot{u}, \tag{21}$$

where n is the normal to the interface, ρ is the fluid density and $\ddot{u}$ is the particle acceleration. Those interface conditions were applied for FSI analyses.

5 Numerical results and discussion

To model an impact to a plate, a simplified numerical model was considered. Instead of direct impact of an object to the plate, a spring-mass model was used in the model. Figure 4 illustrates the model. A linear spring is attached between the single mass and the point of impact of the composite plate. In this study, the impact was assumed at the center of the square plate.

The properties of the composite were provided in Table 1. Both the fiber and matrix material properties were given. The composite plate was 1.0 m × 1.0 m with the thickness of 1.0 mm, and the orientations of the layers were [0°/90°/90°/0°]. The plate was clamped along all the boundaries. The fluid domain had the mass density 1000 kg/m^3 and the speed of sound 1500 m/s. The single mass and the spring

Table 1 Properties of composite

Property	Value
Fiber longitudinal modulus	220 GPa
Fiber transverse modulus	28 GPa
Fiber inplane shear modulus	30 GPa
Fiber inplane Poisson's ratio	0.12
Fiber transverse Poisson's ratio	0.4
Matrix elastic modulus	3.0 GPa
Matrix shear modulus	1.154 GPa
Matrix Poisson's ratio	0.3
Fiber volume fraction	0.5
Fiber failure strain in tension	0.0117
Fiber failure strain in compression	0.0117
Matrix failure strain in tension	0.0066
Matrix failure strain in compression	0.0066
Fiber/matrix interface shear strength	80 MPa
Fiber/matrix interface normal strength	54 MPa

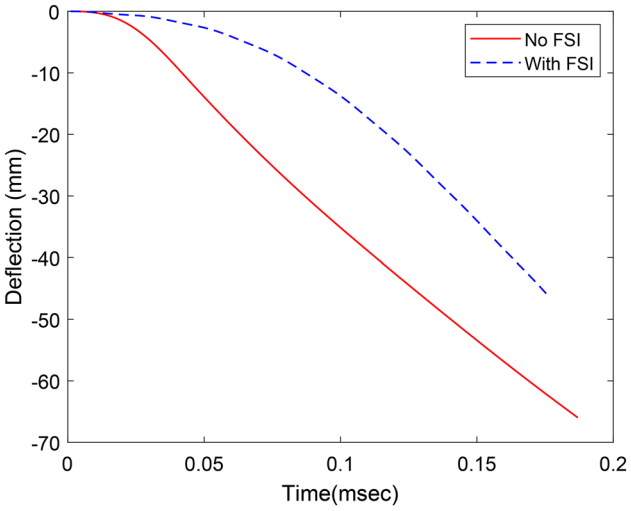

Fig. 5 Comparison of center deflection of the laminated composite plate subjected to simplified impact loading with or without FSI

in Fig. 4 were assumed 100 kg and 2×10^7 N/m. The initial velocity of the mass was also assumed 250 m/s in the downward direction. In the analysis model, if the spring resulted in a tensile force, the spring and mass were ignored for the subsequent calculation because it was considered that the impactor was separated from the plate. Then, no secondary impact was considered, either.

The first study was to compare the dynamic response and failure of the composite plate while the plate had FSI or not under the same loading condition. The simplified impact loading as described above was applied to the composite plate. The plate was divided into 400 elements with a single element through the thickness. The different orientations of the layers were modelled using different material properties at each integration point along the plate thickness. When the plate was supported by water at the back, the boundary of the water was assumed non-reflective, i.e. infifnite, except for the FSI interface.

Figure 5 compares the center deflection of the composite plate under the simplified impact model while the plate was supported by the fluid domain or not, respectively. The fluid domain at the backside of the composite plate reduced the central deflection of the plate under the same impact loading condition. The deflections were plotted until failure of the composite plate. The maximum deflection was about 40% greater for the plate without FSI as compared to that with FSI. The former also showed a faster increase of the central deflection with respect to time.

The major failure occurred at 0.187 ms without FSI and 0.176 ms with FSI. Thus, the FSI resulted in failure about 6% earlier as compared to the no-FSI case. The failure without FSI was more focused around the impact point, and the FSI case yielded a longer extended failure zone than the no-FSI case as shown in Fig. 6 which shows the fiber failure zone at the bottom 0° layer of the cross-ply composite. The orientation of the fibers is in the horizontal axis of the figure. Interestingly, the plate with FSI did not show the failure at the center but a little away from the center. Figure 7 shows the matrix failure zone in the same bottom layer. The matrix failure with FSI was also extended longer along the vertical direction, which is the perpendicular direction to the fibers of the layer.

Computed strains were plotted and compared. Figure 8 shows the locations where strain–time histories were computed. One was next to the center while another was next to the corner of the plate. Figure 9 shows the strain time-history plots of the impacted composite plate without FSI at the selected locations while Fig. 10 shows the strain–time history plots of the same composite with FSI at the same locations. In both figures, the longitudinal normal strain and the shear strain were computed for the fibers on the bottom 0° layer. Comparing the two figures indicated that the strain response next to the center location #44 was similar qualitatively with and without FSI even though their magnitudes were quite different. However, strains at other locations had very different responses because of FSI.

Figures 11 and 12 compare the normal strains along the fiber direction at the locations #33 and #11 with and without FSI. The location #11 is next to the corner of the plate while location #33 closer to the center. As shown in the graphs, the effect of FSI was greater on the strain next to the corner than other locations. The FSI reduced the vibrational motion significantly near the corner area. These observations agreed with the experimental results at least qualitatively (Kwon et al. 2010; Kwon and Plessas 2014; Kwon 2020). Thus,

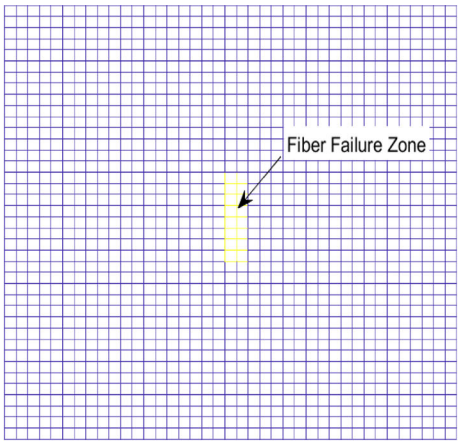

(a) Without FSI

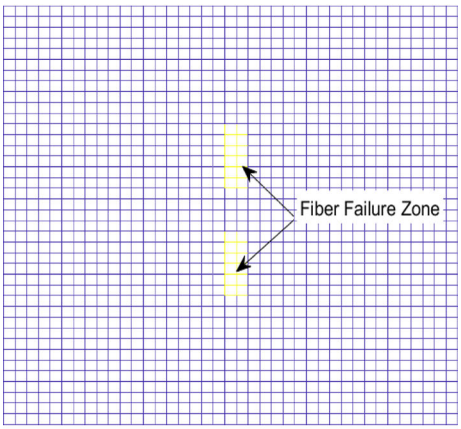

(b) With FSI

Fig. 6 Comparison of fiber failure zone at the bottom 0° layer with impact **a** without and **b** with FSI

(a) Without FSI

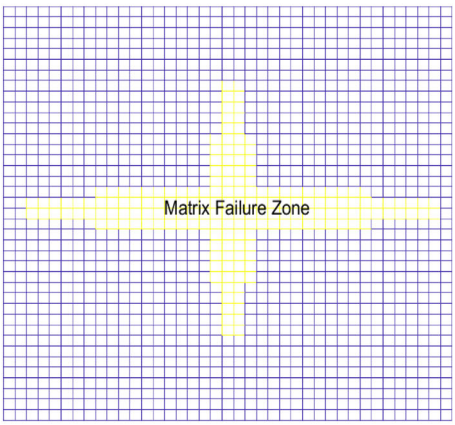

(b) With FSI

Fig. 7 Comparison of matrix failure zone at the bottom 0° layer with impact **a** without and **b** with FSI

the numerical analysis was indirectly validated against the previous experimental results.

The impact loading resulted in different contact loads with the composite plate depending the FSI condition even though the initial impact conditions, like the impact mass and the initial velocity, remained the same. Therefore, the effect of FSI resulted in an earlier failure as compared to the no-FSI case. In the next study, the impact load was replaced by an externally applied concentric load which was a linear function of time. That is, $F(t) = -10^6\, t$ (kN) was applied to the center. The applied force remained the same regardless of the FSI condition. The negative sign denotes the force was applied in the downward direction. Dynamic response and failure were compared as the composite plate was supported by water or not.

Without FSI, the composite plate had the major failure with the concentrated load 117 kN. However, FSI increased the failure load to 241 kN, which was about 200% greater than the failure load without FSI. When comparing the results

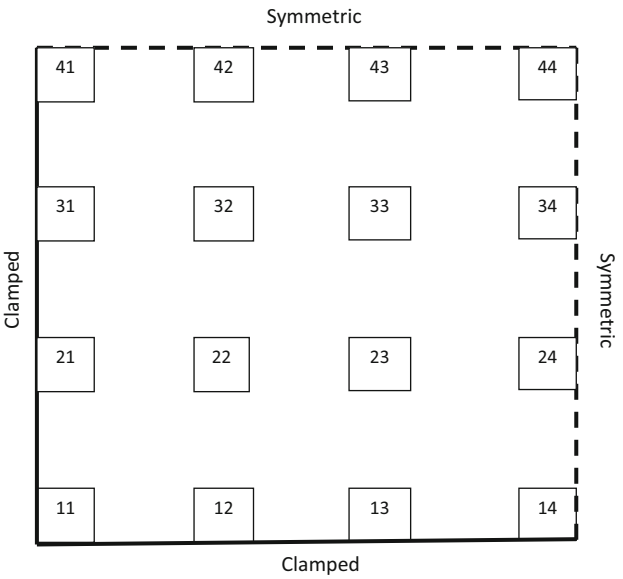

Fig. 8 Element location for strain comparison

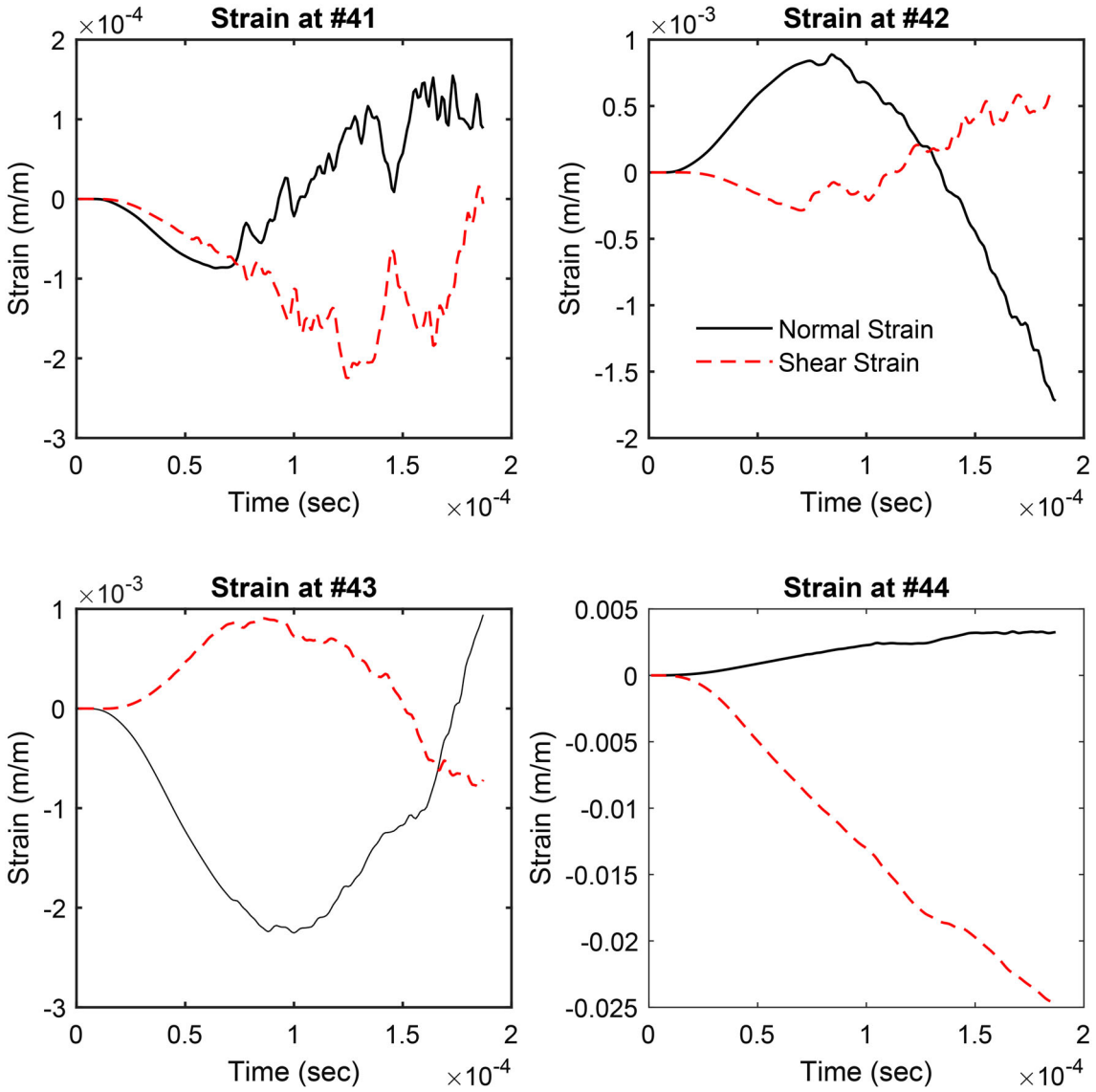

Fig. 9 Strain–time histories of fibers of composite without FSI and subjected to impact

of this and former examples, the effect of FSI was opposite. In the former example, the effect of FSI resulted in earlier failure while it caused later failure for the present example as compared to those without FSI. The difference is the loading condition. When a specified and predetermined force was applied to the composite plate, the FSI gave a positive effect to increase the failure load. On the other hand, the impact loading with the same initial impact condition could produce a greater contact force with FSI, which produced earlier failure of the composite plate. As shown in the experimental study, the failure with FSI occurred with a lower initial velocity of the same impact mass than that for the failure without FSI.

The central deflection for the linearly varying concentrated force was plotted in Fig. 13 with or without FSI. The water reduced the deflection significantly. The maximum deflection at the center was about 50% greater for the no-FSI case than the FSI case even though the failure load was 200% greater for the latter. Figures 14 and 15 compare the longitudinal normal strains of fibers at the locations #22 and #44 of the bottom 0° layer. At the location #22, the strain with FSI was higher than that without FSI, but it was opposite at the location #44. The difference in the strain magnitudes with and without FSI was greater at the location #44, i.e. next to the center of the plate, than at the location #22.

The next study was conducted as a parametric study, in which the fiber volume fraction was varied. The previous study used the fiber volume fraction 0.5. It was decreased to 0.4 and increased to 0.6. However, the density of the composite was not changed. As the fiber volume fraction changes,

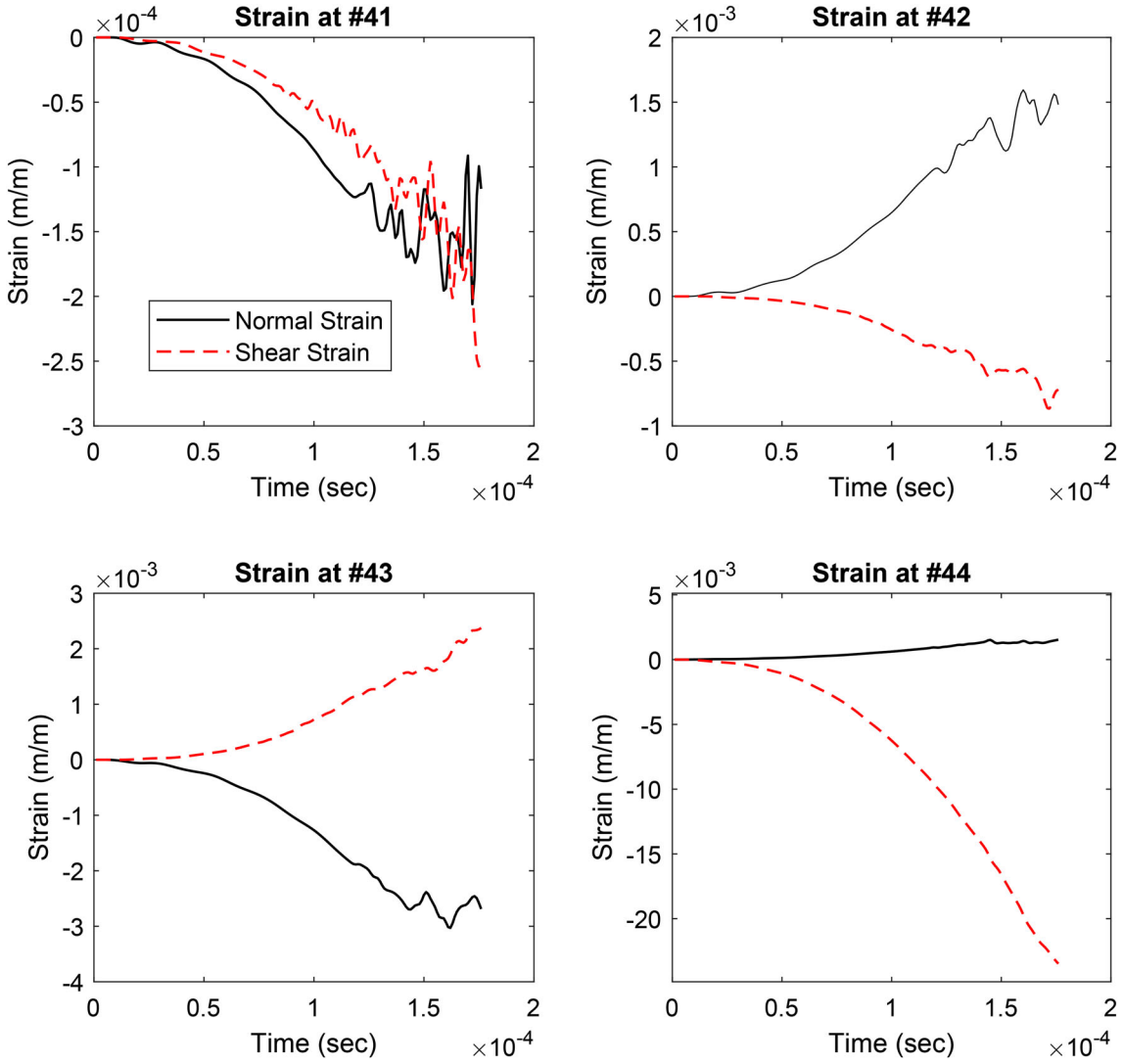

Fig. 10 Strain–time histories of fibers of composite with FSI and subjected to impact

the overall stiffness of the plate also changes. That results in a change in their vibrational frequencies and dynamic responses. In addition, the load-bearing portions by the fibers and the matrix were also affected, which resulted in different failure loads.

The time-histories of the longitudinal normal strains in the fibers of the bottom layer were compared among different fiber volume fractions at different locations as shown in Figs. 16, 17, 18. The strain next to the center of the plate was compared in Fig. 16, which shows the strain response is very close among different fiber volume fraction cases. The fiber volume of 0.4 resulted in failure at the latest time, which means the highest load, while the case of fiber volume 0.6 had the earliest failure among the three cases. Table 2 shows the failure loads for different fiber volume fractions and the conditions of FSI. The results suggested that the failure load increased or decreased by about 7% as the fiber volume fraction was varied from 0.5 to 0.4 or 0.6.

Unlike the location #44, the strains at locations #22 and #11 were quite different depending on the fiber volume fraction. The case of the fiber volume fraction 0.4 yielded the maximum strain at the location #22, while the case of 0.5 gave the maximum strain at the location #11. Especially, strain response next to the corner location #11 was very drastically different as the fiber volume fraction was varied.

Another parametric study was a change in the fiber orientation. In this study, both top and bottom 0° layers were oriented to 5°, respectively. Figures 19 and 20 are the plots of fiber strains at the location #44 and #33, respectively. The longitudinal fiber strain was significantly influenced by the angle change of the outer layers at the location #44. The normal strain became compressive with the layer angle 5°. On the other hand, the strain at #33 did not show any major

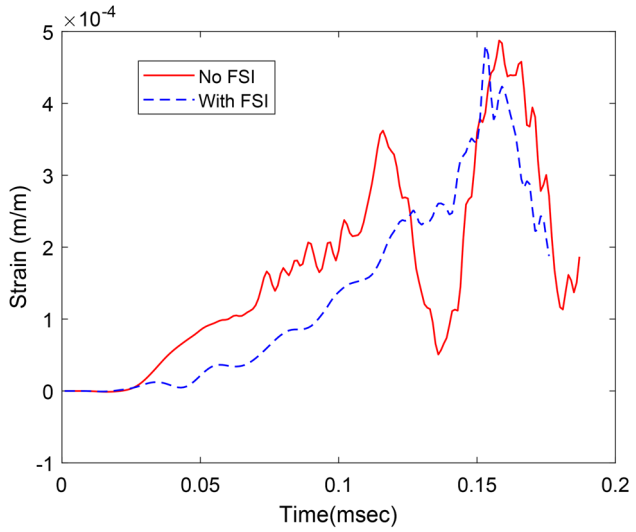

Fig. 11 Normal strain ε_x time history at the location #33 of the composite plate with or without FSI and subjected to impact

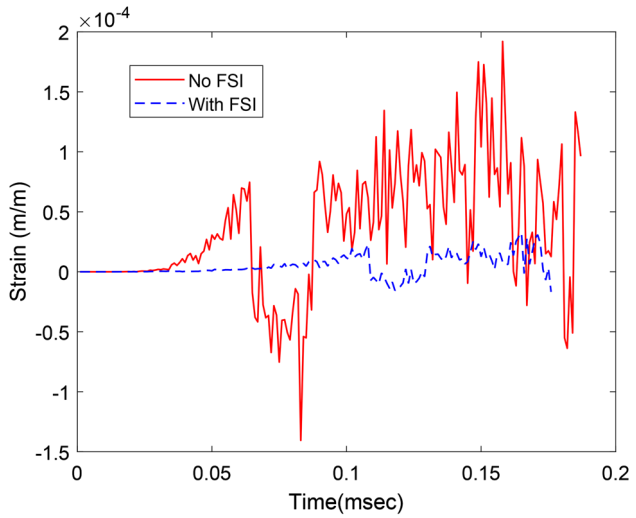

Fig. 12 Normal strain ε_x time history at the location #11 of the composite plate with or without FSI and subjected to impact

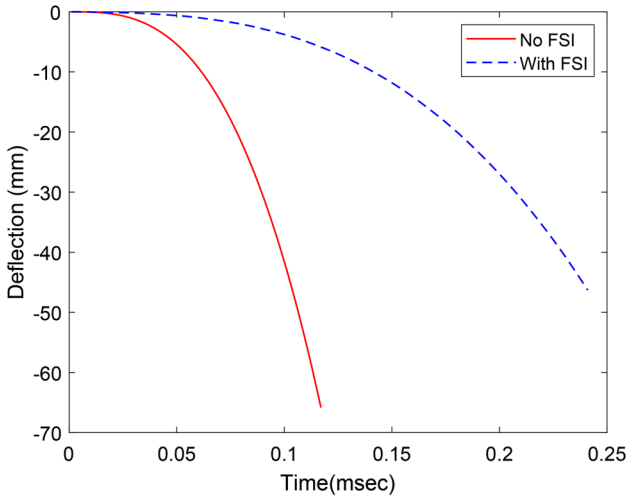

Fig. 13 Center deflection of the composite plate with or without FSI and subjected to linearly varying concentrated force

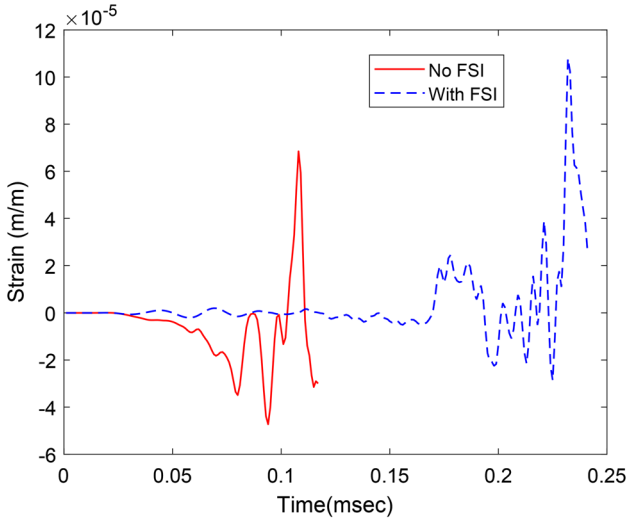

Fig. 14 Normal strains ε_x at the location #22 of the composite plate with or without FSI and subjected to linearly varying concentrated force

change. Only the magnitude of the fiber strain was affected by the layer orientation.

6 Conclusions

A series of numerical studies were conducted to investigate the effect of FSI on dynamic response and failure of a laminated composite plate supported by a fluid medium, water in this study. The multiscale-based composite failure criteria were utilized to predict failures in the analysis. A proper coupling procedure was applied to solve the finite element model for the composite structure and the cellular automata technique for the fluid domain together.

First, a simplified impact model was considered for a cross-ply composite plate. When the composite plate was supported by water with FSI, the same initial condition for the impact loading resulted in earlier failure of the composite plate because of the greater contact force between the plate and the impact mass. This result agreed qualitatively with the experimental test data in the previous studies. The next study applied a linear varying concentrated force at the center of the cross-ply composite. For this case, FSI resulted in a higher failure load as compared to the dry plate without FSI.

Thus, the failure of FSI was dependent on the loading type. The predetermined loading increased the failure load because of FSI, while the impact-type loading reduced the failure load due to FSI. The latter type of loading is a more typical external loading. In that case, design of a composite

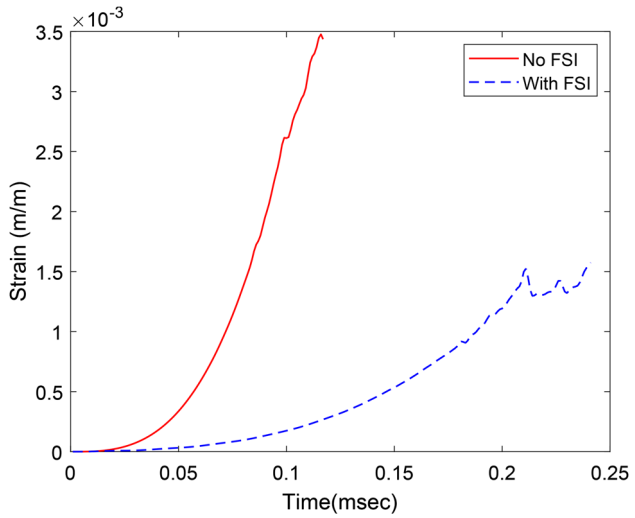

Fig. 15 Normal strains ε_x at the location #44 of the composite plate with or without FSI and subjected to linearly varying concentrated force

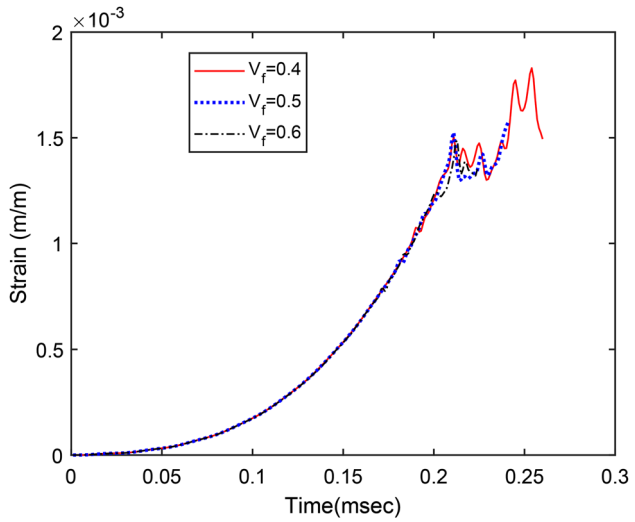

Fig. 16 Comparison of normal fiber strains at the location #44 of the composite plate with FSI and subjected to linearly varying concentrated force for different fiber volume fractions

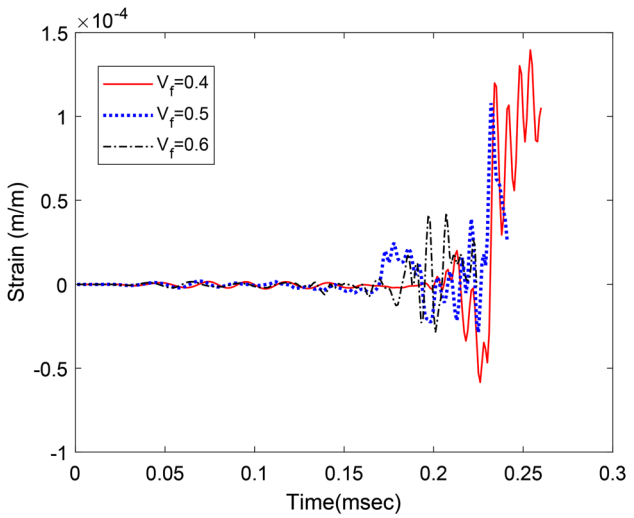

Fig. 17 Comparison of normal fiber strains at the location #22 of the composite plate with FSI and subjected to linearly varying concentrated force for different fiber volume fractions

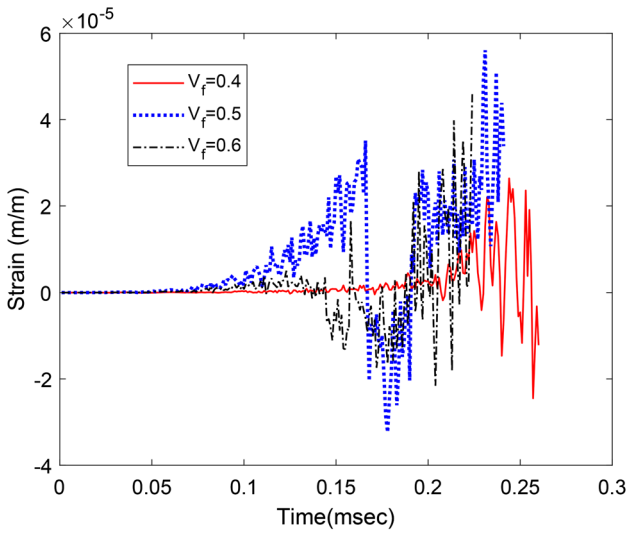

Fig. 18 Comparison of normal fiber strains at the location #11 of the composite plate with FSI and subjected to linearly varying concentrated force for different fiber volume fractions

structure without considering FSI could lead to a premature failure when the structure was applied to offshore and marine applications.

A series of parametric study suggested that the effect of the change in the fiber volume fraction or layer orientation influenced the dynamic response of the plate. At some locations, such a change in a parameter did not show a sizable effect while there was a significant effect at other locations. Thus, the effect was very dependent on the location of the structure.

In summary, the FSI with composite structures influenced the failure loads of the structures as compared to the same structures without FSI. In practical applications such as

Table 2 Comparison of failure load for linearly varying concentrated force

Fiber vol. frac.	With FSI (kN)	% in change (%)	No FSI (kN)	% in change (%)
0.4	260	7.9	125	6.8
0.5	241	0.0	117	0.0
0.6	224	− 7.1	109	− 6.8

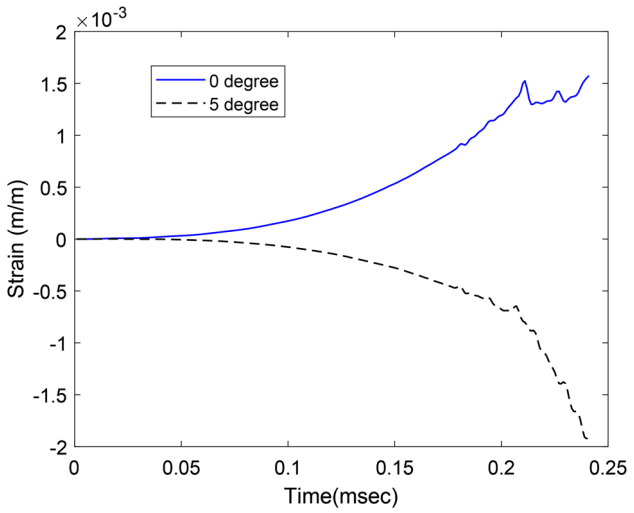

Fig. 19 Comparison of fiber normal strains at the location #44 of the bottom layer of cross-ply plate with FSI as the fiber orientation was varied

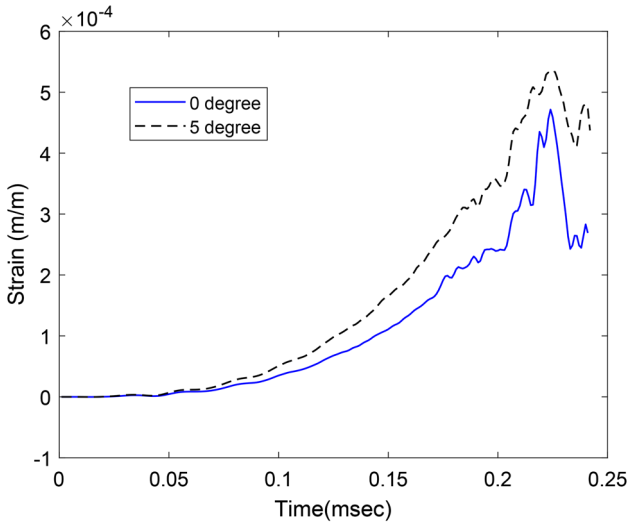

Fig. 20 Comparison of fiber normal strains at the location #33 of the bottom layer of cross-ply plate with FSI as the fiber orientation was varied

impact loading, the failure could occur prematurely if the FSI was not considered in the design and analysis. The effects of FSI were different depending on the locations of the structure because the effect was not uniform over the entire structure.

Acknowledgements The author acknowledges the financial support from Office of Naval Research (ONR).

Compliance with ethical standards

Conflict of interest The author states there is no conflict of interest.

References

Abrate S (1994) Impact on laminated composites; recent advances. Appl Mech Rev 47(11):517–544

Alaei D, Kwon YW, Ramezani A (2019) Fluid-structure interaction on concentric composite cylinders containing fluids in the annulus. Multiscale Multidiscipl Model Exp Design 2(3):185–197

Aslan Z, Karakuzu R, Okutan B (2003) The response of laminated composite plates under low-velocity impact loading. Compos Struct 59:119–127

Chen W, Haroun MA, Liu F (1996) Large amplitude liquid sloshing in seismically excited tanks. Earthq Eng Struct Dyn 25(7):653–669

Craugh LE, Kwon YW (2013) Coupled finite element and cellular automata methods for analysis of composite structures with fluid-structure interaction. Compos Struct 102:124–137

Di Martino ES, Guadagni G, Fumero A, Ballerini G, Spirito R, Biglioli P, Redaelli A (2001) Fluid-structure interaction within realistic three-dimensional models of the aneurysmatic aorta as a guidance to assess the risk of rupture of the aneurysm. Med Eng Phys 23:647–655

Hosur MV, Jain K, Chowdhury F, Jeelani S, Bhat MR, Murthy CRL (2007) Low velocity impact response of carbon/epoxy laminates subjected to cold-dry and cold-moist conditioning. Compos Struct 79:300–311

Karamanos SA, Patkas LA, Platyrrachos MA (2006) Sloshing effects on the seismic design of horizontal-cylindrical and spherical industrial vessels. ASME J Pressure Vessel Technol 128(3):328–340

Kwon YW (2013) Analysis of laminated and sandwich composite structures using solid-like shell elements. Appl Compos Mater 20(4):355–373

Kwon YW (2014) Dynamic responses of composite structures in contact with water while subjected to harmonic loads. Appl Compos Mater 21(1):227–245

Kwon YW (2016) Multiphysics and multiscale modeling: techniques and application. CRC Press, Boca Raton

Kwon YW (2017) Finite difference based cellular automaton technique for structural and fluid-structure interaction applications. ASME J Pressure Vessel Technol 139:041301

Kwon YW (2020) Fluid-structure interaction of composite structures. Springer-Nature, Berlin

Kwon YW, Bang H-C (2000) Finite element method using MATLAB, 2nd edn. CRC Press, Boca Raton

Kwon YW, Bowling JD (2018) Dynamic responses of composite structures coupled through fluid medium. Multiscale Multidiscipl Model Exp Design 1(1):69–82

Kwon YW, Conner RP (2012) Low velocity impact on polymer composite plate in contact with water. Int J Multiphys 6(3):179–197

Kwon YW, Darcy J (2018a) Failure criteria for fibrous composites based on multiscale modeling. Multiscale Multidiscipl Model Exp Design 1(1):3–17

Kwon YW, Darcy J (2018b) Further discussion on newly developed failure criteria for fibrous composites. Multiscale Multidiscipl Model Exp Design 1(4):307–316

Kwon YW, Fox PK (1993) Underwater shock response of a cylinder subjected to a side on explosion. Comput Struct 48(4):637–646

Kwon YW, Kim C (1998) Micromechanical model for thermal analysis of particulate and fibrous composites. J Therm Stresses 21:21–39

Kwon YW, Panick CJ (2020) "Strain rate dependent failure criteria for fibrous composites using multiscale approach. Multiscale Multidiscipl Model Exp Design 3:11–22

Kwon YW, Park MS (2013) Versatile micromechanics model for multiscale analysis of composite structures. Appl Compos Mater 20(4):673–692

Kwon YW, Plessas SD (2014) Numerical modal analysis of composite structures coupled with water. Compos Struct 116:325–335

Kwon KW, Violette MA (2012) Damage initiation and growth in laminated polymer composite plates with fluid-structure interaction under impact loading. Int J Multiphys 6(1):29–42

Kwon YW, Owens AC, Kwon AS, Didoszak JM (2010) Experimental study of impact on composite plates with fluid-structure interaction. Int J Multiphys 4(3):259–271

Kwon YW, Violette MA, McCrillis RD, Didoszak JM (2012) Transient dynamic response and failure of sandwich composite structures under impact loading with fluid structure interaction. Appl Compos Mater 19(6):921–940

Kwon YW, Priest EM, Gordis JH (2013) Investigation of vibrational characteristics of composite beams with fluid-structure interaction. Compos Struct 105:269–278

Kwon YW, Teo HF, Park C (2016) Cyclic loading on composite beams with fluid structure interaction. Exp Mech 56(4):645–652

Kwon YW, South T, Yun KJ (2017) Low velocity impact to composite box containing water and baffles, composite structures. ASME J Pressure Vessel Technol 139(3):031304

Simsek FG, Kwon YW (2015) Investigation of material modeling in fluid-structure interaction analysis of an idealized three-layered abdominal aorta: aneurysm initiation and fully developed aneurysm. J Biol Phys 41(2):173–201

Strait LH, Karasek ML, Amateau MF (1992) Effects of stacking sequence on the impact resistance of carbon fiber reinforced thermoplastic toughened epoxy laminates. J Compos Mater 26(12):1725–1740

Weaver DS, Ziada S, Au-Yang MK, Chen SS, Païdoussis MP, Pettigrew MJ (2000) Flow-induced vibrations in power and process plant components—progress and prospects. ASME J Pressure Vessel Technol 122:339–348